

Optimal control of connected autonomous vehicles in a mixed traffic corridor

Wenbo Sun, Fangni Zhang

Department of Industrial and Manufacturing Systems Engineering, University of Hong Kong, Hong Kong

Wei Liu, and Qingying He

Department of Aeronautical and Aviation Engineering, The Hong Kong Polytechnic University, Hong Kong, China

APPENDIX A NOTATION LIST

TABLE A1
NOTATION LIST

| Variable | Description |
|---------------|--|
| t | Time |
| T_{OH} | Length of the optimization horizon |
| T_{UD} | Update frequency of the optimal control |
| d_{start} | Start position of the control corridor |
| d_{end} | End position of the control corridor |
| $n(t)$ | The number of vehicles in the control traffic stream |
| $N(t)$ | Set of all vehicles in the control traffic stream at time t |
| $N_c(t)$ | Set of CAVs in $N(t)$ |
| $N_h(t)$ | Set of HVs in $N(t)$ |
| t_0, t_f | Start time and end time of the optimization horizon, respectively |
| d_{sig} | Location of the intersection (if exists) |
| $sig(t)$ | Phase of the signal at time t (if exists) |
| t_r, t_g | Durations of red and green phases, respectively (if exists) |
| J | Objective function |
| Φ | Final cost function on travel distance in the objective function |
| \mathcal{L} | Energy consumption function in the objective function |
| w_1, w_2 | Weighting factors for travel distance and energy consumption, respectively |
| w_3, w_4 | Weighting factors to penalize violating car-following model and safety constraints, respectively |
| \mathcal{H} | Hamiltonian function |
| $\lambda(t)$ | Co-state related to state $x(t)$ |
| $u(t)$ | Control input denoting acceleration of all CAVs in the control traffic stream at time t |
| $s_i(t)$ | Slack variable for HV i at time t in the car-following model |
| $l_i(t)$ | Slack variable for vehicle i at time t in the safety constraint |
| p_i | Binary variable, 1 if vehicle i can pass the intersection, and 0 otherwise |
| M | A sufficiently large value in signal constraints with the Big-M method |
| L | Vehicle length |
| $d_i(t)$ | Location of vehicle i at time t |
| $v_i(t)$ | Speed of vehicle i at time t |
| $a_i(t)$ | Acceleration of vehicle i at time t |
| $x(t)$ | State of all vehicles in the control traffic stream at time t |
| h | Time headway for a safe car-following distance |
| h_{min} | Minimum following distance when the vehicle is stationary |
| v_{max} | Maximum speed |
| v_{min} | Minimum speed |
| a_{max} | Maximum acceleration |
| a_{min} | Minimum acceleration |
| τ | Adaptation time of the following vehicle to reach the speed of its preceding vehicle |
| v_0 | Desired speed of vehicles in the IDM model |
| s_0 | Minimum spacing between two vehicles in the IDM model |
| δ | Acceleration exponent in the IDM model |
| a, b | Vehicle maximum acceleration and comfortable deceleration in the IDM model, respectively |
| T_G | Time gap in the IDM |
| η | Engine efficiency in transferring energy |

APPENDIX B COMPARISON OF DIFFERENT WEIGHTING FACTORS FOR TRAVEL DISTANCE AND ENERGY CONSUMPTION

In Section III, we evaluate the proposed control framework with normalized weighting factors presented in Section II-A. Let \bar{w}_1 and \bar{w}_2 denote the normalized weighting factors, we compare the performance of the proposed methods with 5 different combinations of weighting factors shown in Table A2. Specifically, the third case is the same as the numerical results in Section III, i.e., the normalized weighting factors. Based on the third case, reducing energy consumption is more important in the first two cases while improving the travel distance is more essential in the last two cases. For fairness, the numerical results are conducted in a signalized scenario presented in Section III-A with traffic demand set at 500 vehicles per hour. Moreover, the permutation of controllable CAVs is fixed, where 10 controllable CAVs are evenly distributed in the traffic flow of 50 vehicles (20% controllable vehicles).

Fig. A1 and Table A2 show the results with different weighting factors for travel distance and energy consumption. The normalized energy consumption is presented in the table to make a fair comparison of all cases, and the tractive energy consumption is also presented in the table for reference. As shown in Table A2, when the optimal control emphasizes more on improving the travel distance (w_1 increases or w_2 decreases), the traffic throughput of the control corridor is improved (e.g., the travel time decreases and the average leaving speed increases comparing case W1 with case W3), and the normalized energy consumption increases (e.g., case W3 and case W5). It is also noted that compared with case W3, normalized energy consumption increases even if the proposed method emphasizes more on energy consumption in case W1. This is because controllable CAVs will avoid acceleration and deacceleration if optimal control only considers reducing energy consumption. However, in the presence of the red signal, all vehicles have to stop. Although controllable CAVs can guide following vehicles to smoothly reduce speeds, they will also adopt smaller acceleration after the signal turns green. Therefore, for case W1 shown in Fig. A1(a), the average speed of all vehicles leaving the control corridor is low, which reduces the road throughput (longer travel time). Moreover, the lower average speed has a larger kinetic energy gap, resulting in more normalized energy consumption. Overall, the numerical results in Table A2 show that the normalized weighting factors used in Section III can make a balance between road throughput and energy consumption.

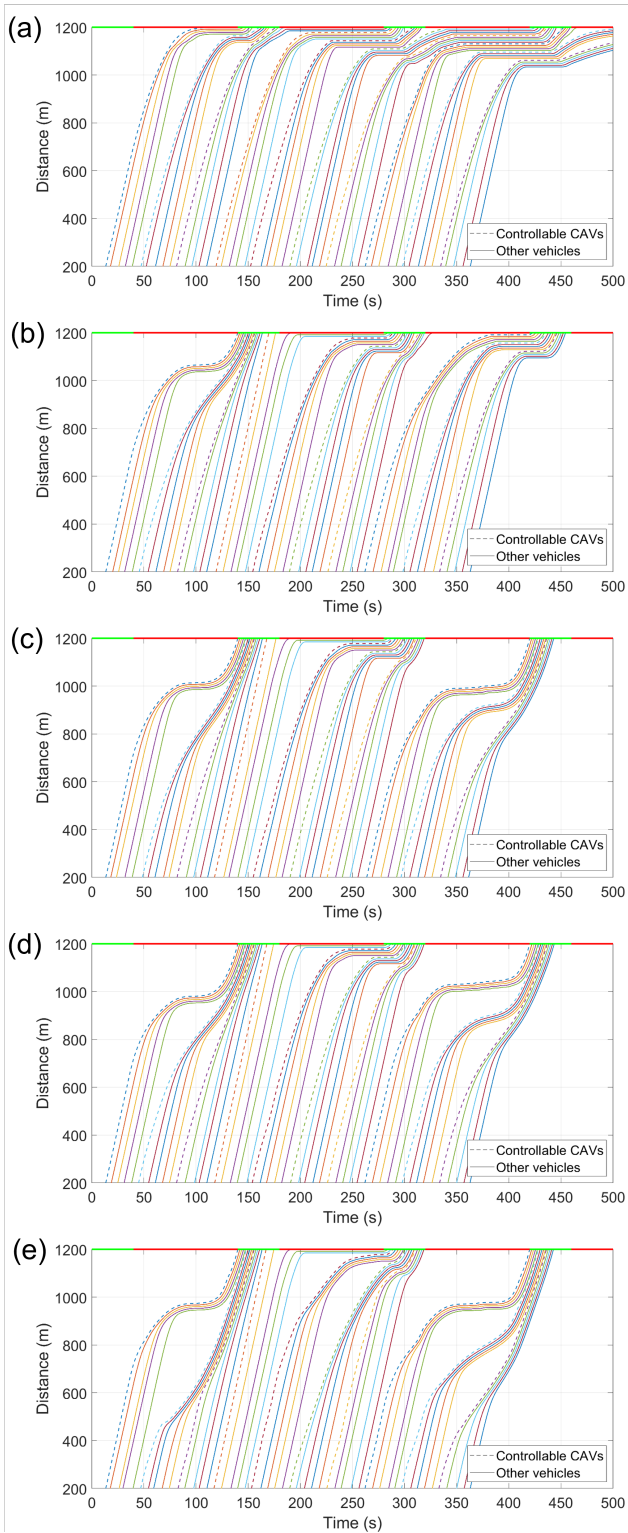


Fig. A1. Trajectories of vehicles with different weighting factors (20% controllable CAVs). (a) Case W1. (b) Case W2. (c) Case W3. (d) Case W4. (e) Case W5.

TABLE A2
PERFORMANCE OF DIFFERENT WEIGHTING FACTORS

| Fig. A1 Case name | w_1 | w_2 | Travel time (s) | Normalized energy (MJ) | Traction energy (MJ) | Average leaving speed (m/s) |
|-------------------|-----------------------|-----------------------|-----------------|------------------------|----------------------|-----------------------------|
| (a) W1 | 0 | \bar{w}_2 | 163.19 | 5.19 | 3.96 | 4.80 |
| (b) W2 | $\frac{\bar{w}_1}{2}$ | \bar{w}_2 | 108.23 | 4.34 | 3.43 | 10.65 |
| (c) W3 | \bar{w}_1 | \bar{w}_2 | 103.46 | 4.35 | 3.68 | 13.62 |
| (d) W4 | \bar{w}_1 | $\frac{\bar{w}_2}{2}$ | 103.78 | 4.40 | 3.73 | 13.67 |
| (e) W5 | \bar{w}_1 | 0 | 103.58 | 4.67 | 4.05 | 14.10 |

APPENDIX C PROOF OF PROPOSITION 1

Proof. (19) can be obtained according to (12)–(18) with $w_{22} = 0$.

According to (19), $\dot{a}_1(t) = -\frac{w_{11}+w_{12}-w_{12}e^{(t-t_f)/\tau}}{2w_{21}} < 0$ and $a_1(t_f) = 0$. Therefore, $a_1(t)$ is non-negative but keeps decreasing during the optimization horizon, and thus we have Proposition 1(i) and (ii).

Proposition 1(iii) can be obtained by noting $\frac{\partial a_1(t)}{\partial w_{11}} \geq 0$, $\frac{\partial a_1(t)}{\partial w_{12}} \geq 0$ and $\frac{\partial a_1(t)}{\partial w_{21}} \leq 0$. This completes the proof. \square

APPENDIX D ANALYTICAL SOLUTION WITH $a_1(t) = At + B + Ce^{Dt}$ IN THE TWO-VEHICLE SCENARIO

This appendix derives the optimal control shown in (21)–(22) assuming $a_1(t) = At + B + Ce^{Dt}$ with unspecified coefficients A, B, C, D .

A, B, C, D can be solved from (12)–(18). Specifically, with known $a_1(t)$, $\lambda_2(t)$ can be obtained according to (12). Then, $\lambda_4(t)$ can be solved from (15) (17), and (18). Further, we can obtain $a_2(t)$ from either (15) or (17). The unspecified coefficients A, B, C, D in $a_2(t)$ should satisfy the GHR model presented in (13), where speeds of two vehicles can be obtained by integrating the associated accelerations, i.e., $v_{\{1,2\}}(t) = v_{\{1,2\}}(t_0) + \int_{t_0}^t a_{\{1,2\}}(t')dt'$. Detailed process is shown below.

Given $a_1(t) = At + B + Ce^{Dt}$ and according to (12), $\lambda_2(t)$ can be written as:

$$\lambda_2(t) = -2w_{21}(At + B + Ce^{Dt}). \quad (\text{A1})$$

The derivative of (A1) with respect to time t is:

$$\dot{\lambda}_2(t) = -2w_{21}(A + CD)e^{Dt}. \quad (\text{A2})$$

Combining (15) and (17) gives $\dot{\lambda}_4(t) + \dot{\lambda}_2(t) = w_{11} + w_{12}$. Thus, $\lambda_4(t)$ can be solved by integrating $\dot{\lambda}_4(t)$ and letting it satisfy (18):

$$\lambda_4(t) = (w_{11} + w_{12})(t - t_f) + 2w_{21}(At + B + Ce^{Dt}). \quad (\text{A3})$$

With known $\dot{\lambda}_2(t)$ and $\lambda_4(t)$, $a_2(t)$ can be solved according to (15), which is:

$$a_2(t) = \frac{1}{2w_{22}} \left[\tau w_{11} - (w_{11} + w_{12})(t - t_f) - 2w_{21}(At + B + Ce^{Dt}) + 2\tau w_{21}(A + CD)e^{Dt} \right]. \quad (\text{A4})$$

Meanwhile, $v_1(t)$ and $v_2(t)$ can be obtained by integrating $a_1(t)$ and $a_2(t)$ while satisfying the initial states $v_1(0)$ and $v_2(0)$, respectively. Then, according to the GHR model shown in (4), $a_2(t)$ can also be written as:

$$a_2(t) = (v_1(t) - v_2(t)) / \tau \quad (\text{A5})$$

In this case, A, B, C, D can be solved by ensuring right hand sides of (A4) and (A5) equal, which is shown below:

$$\begin{aligned} \frac{1}{2w_{22}} & \left[\tau w_{11} + 2\tau w_{21}(A + C e^{Dt}) - (w_{11} + w_{12})(t - t_f) \right. \\ & - 2w_{21}(At + B + C e^{Dt}) \Big] = -\frac{1}{2w_{22}} \left[w_{11}t \right. \\ & + 2w_{21}(At + C e^{Dt} - C) \Big] + \frac{1}{\tau} \left[v_1(0) - v_2(0) \right. \\ & + (1/2At^2 + Bt + C(e^{Dt} - 1)/D)(1 + w_{21}/w_{22}) \\ & \left. \left. + \frac{w_{11} + w_{12}}{2w_{22}}(1/2t^2 - t_f t) \right] \right]. \end{aligned} \quad (\text{A6})$$

In case of $w_{22} \neq 0$, parts of undetermined coefficients (A, B, D) can be solved by letting first-order, second-order and exponential terms equal on the right and the left hand side of (A6). C is determined by (18). The solved A, B, C, D are:

$$A = -\frac{w_{11} + w_{12}}{2(w_{21} + w_{22})}, \quad (\text{A7})$$

$$B = \frac{(w_{11} + w_{12})t_f - w_{12}\tau}{2(w_{21} + w_{22})}, \quad (\text{A8})$$

$$C = e^{-\sqrt{\frac{w_{21}+w_{22}}{\tau^2 w_{21}}} t_f} \frac{w_{12}\tau}{2(w_{21} + w_{22})}, \quad (\text{A9})$$

$$D = \sqrt{\frac{w_{21} + w_{22}}{\tau^2 w_{21}}}. \quad (\text{A10})$$

Meanwhile, equalizing the constant terms in (A6) gives:

$$\begin{aligned} \frac{v_1(0) - v_2(0)}{\tau} &= \frac{\tau w_{11} + (w_{11} + w_{12})t_f}{2(w_{21} + w_{22})} + \\ & \frac{w_{12}\tau}{2w_{22}} e^{-\sqrt{\frac{w_{21}+w_{22}}{\tau^2 w_{21}}} t_f} \left[\sqrt{\frac{w_{21}}{w_{21} + w_{22}}} - \frac{w_{21}}{w_{21} + w_{22}} \right]. \end{aligned} \quad (\text{A11})$$

Let φ represent the right hand side of (A11). We can verify that $\varphi > 0$ because $0 \leq \frac{w_{21}}{w_{21} + w_{22}} \leq 1$, i.e., (22). To sum up, with (A11) being satisfied, the analytical solution (21) can be derived explicitly from (A7)–(A10).

APPENDIX E PROOF OF LEMMA 1

Proof. According to the GHR model, the following vehicle will have zero acceleration as long as it reaches the same speed as its preceding CAV. With a higher initial speed and non-negative acceleration, the lead CAV will always drive at a higher speed compared with the following vehicle, i.e., $v_1(t) \geq v_2(t)$ for all $t \in [t_0, t_f]$. Thus, two vehicles will not collide as the distance between two vehicles is non-decreasing during the optimization horizon $[0, t_f]$. This completes the proof. \square

APPENDIX F PROOF OF REMARK 1

Proof. Taking derivative of (21) with respect to time t gives:

$$\begin{aligned} \dot{a}_1(t) &= -\frac{w_{11} + w_{12}}{2(w_{21} + w_{22})} \\ & + \frac{w_{12}}{2\sqrt{(w_{21} + w_{22})w_{21}}} e^{\sqrt{\frac{w_{21}+w_{22}}{\tau^2 w_{21}}}(t-t_f)}, \end{aligned} \quad (\text{A12})$$

which increases over time t . When $t = t_f$, $\dot{a}_1(t_f) = \frac{-w_{11}-w_{12}+\sqrt{\frac{w_{21}+w_{22}}{w_{21}}}}{2(w_{21}+w_{22})}$. We can verify that $\dot{a}_1(t) \leq \dot{a}_1(t_f) \leq 0$ if $\sqrt{\frac{w_{21}+w_{22}}{w_{21}}} \leq \frac{w_{11}+w_{12}}{w_{12}}$, i.e., the acceleration is non-increasing during the optimization horizon. Moreover, as $a_1(t_f) = 0$, $a_1(t)$ is non-negative for all $t \in [0, t_f]$. This completes the proof. \square

APPENDIX G PROOF OF REMARK 2

Proof. Taking derivative of $a_1(t)$ with respect to w_{11} gives:

$$\frac{\partial a_1(t)}{\partial w_{11}} = \frac{t_f - t}{2(w_{21} + w_{22})} \geq 0. \quad (\text{A13})$$

Therefore, $a_1(t)$ increases with a larger w_{11} , i.e., the first part of Remark 2(i).

Taking derivative of $a_1(t)$ with respect to w_{12} gives:

$$\begin{aligned} \frac{\partial a_1}{\partial w_{12}} &= \frac{t_f - t}{2(w_{21} + w_{22})} \\ & + \frac{\tau}{2(w_{21} + w_{22})} \left[e^{\sqrt{\frac{w_{21}+w_{22}}{\tau^2 w_{21}}}(t-t_f)} - 1 \right]. \end{aligned} \quad (\text{A14})$$

Then, $\frac{\partial^2 a_1}{\partial w_{12} \partial t}$ can be calculated as:

$$\begin{aligned} \frac{\partial^2 a_1}{\partial w_{12} \partial t} &= \frac{-1}{2(w_{21} + w_{22})} \\ & + \frac{\sqrt{\frac{w_{21}+w_{22}}{w_{21}}}}{2(w_{21} + w_{22})} e^{\sqrt{\frac{w_{21}+w_{22}}{\tau^2 w_{21}}}(t-t_f)}, \end{aligned} \quad (\text{A15})$$

which increases with respect to time t . Noting that $\frac{\partial^2 a_1(0)}{\partial w_{12} \partial t} < 0$ and $\frac{\partial^2 a_1(t_f)}{\partial w_{12} \partial t} > 0$, $\frac{\partial a_1(0)}{\partial w_{12}}$ will decrease firstly and then increase with respect to time t . Moreover, as $\frac{\partial a_1(0)}{\partial w_{12}} > 0$ and $\frac{\partial a_1(t_f)}{\partial w_{12}} = 0$, $\frac{\partial a_1(t)}{\partial w_{12}}$ will be positive firstly and then negative in the optimization horizon $[0, t_f]$. In other words, with the increase of w_{12} , the acceleration of the lead CAV would increase firstly during the optimization horizon, but decrease at the later stage of the optimization horizon, i.e., Remark 2(ii).

Taking derivative of $a_1(t)$ with respect to w_{21} gives:

$$\begin{aligned} \frac{\partial a_1}{\partial w_{21}} &= \frac{(w_{11} + w_{12})(t - t_f)}{2(w_{21} + w_{22})^2} + \frac{w_{12}\tau}{2(w_{21} + w_{22})^2} \\ & \left[1 - e^{\sqrt{\frac{w_{21}+w_{22}}{\tau^2 w_{21}}}(t-t_f)} \left(1 + \frac{w_{22}}{w_{21}} \sqrt{\frac{w_{21} + w_{22}}{\tau^2 w_{21}}}(t - t_f) \right) \right]. \end{aligned} \quad (\text{A16})$$

Further, taking derivative of (A16) with respect to time t gives:

$$\frac{\partial^2 a_1}{\partial w_{21} \partial t} = \frac{(w_{11} + w_{12})}{2(w_{21} + w_{22})^2} - \frac{w_{12}\sqrt{\frac{w_{21}+w_{22}}{w_{21}}}}{2(w_{21} + w_{22})^2} \cdot e^{\sqrt{\frac{w_{21}+w_{22}}{\tau^2 w_{21}}}(t-t_f)} \left[1 + \frac{w_{22}}{w_{21}} \sqrt{\frac{w_{21}+w_{22}}{\tau^2 w_{21}}} (t-t_f) + \frac{w_{22}}{2w_{21}} \right]. \quad (\text{A17})$$

Note that the first term in (A17) is constant, whereas the second term will decrease firstly and then increase with respect to time t . Therefore, $\frac{\partial a_1(t)}{\partial w_{22}}$ gets the minimum value at either $t = 0$ or $t = t_f$. Since $\frac{\partial^2 a_1(0)}{\partial w_{21} \partial t} > 0$, we can discuss $\frac{\partial^2 a_1(t_f)}{\partial w_{21} \partial t}$ in two cases. On the one hand, if $\frac{\partial^2 a_1(t_f)}{\partial w_{21} \partial t} \geq 0$, $\frac{\partial^2 a_1}{\partial w_{21} \partial t} \geq \min \left\{ \frac{\partial^2 a_1(0)}{\partial w_{21} \partial t}, \frac{\partial^2 a_1(t_f)}{\partial w_{21} \partial t} \right\} \geq 0$, i.e., $\frac{\partial a_1}{\partial w_{21}}$ increases with respect to time t . Therefore, $\frac{\partial a_1(t)}{\partial w_{21}} \leq \frac{\partial a_1(t_f)}{\partial w_{21}} = 0$. In other words, the acceleration of the lead CAV would decrease with a larger w_{21} . On the other hand, if $\frac{\partial^2 a_1(t_f)}{\partial w_{21} \partial t} < 0$, $\frac{\partial a_1(t)}{\partial w_{21}}$ would increase firstly then decrease with respect to time t . Since $\frac{\partial a_1(0)}{\partial w_{21}} < 0$ (with a sufficiently large t_f) and $\frac{\partial a_1(t_f)}{\partial w_{21}} = 0$, $\frac{\partial a_1(t)}{\partial w_{21}}$ would be negative firstly and then positive in the optimization horizon, i.e., Remark 2(iii).

Taking derivative of $a_1(t)$ with respect to w_{22} gives:

$$\begin{aligned} \frac{\partial a_1}{\partial w_{22}} = & \frac{-1}{2(w_{21} + w_{22})^2} \left[(w_{11} + w_{12})(t_f - t) \right. \\ & + w_{12}\tau \left(e^{\sqrt{\frac{w_{21}+w_{22}}{\tau^2 w_{21}}}(t-t_f)} - 1 \right) \left. \right] \\ & + \frac{w_{12}e\sqrt{\frac{w_{21}+w_{22}}{\tau^2 w_{21}}}(t-t_f)}{4(w_{21} + w_{22})^2} \sqrt{\frac{w_{21}+w_{22}}{w_{21}}}(t-t_f). \end{aligned} \quad (\text{A18})$$

As the first term has the same sign as $(-a_1(t))$ which is non-positive and the second term in (A18) is also non-positive, we have $\frac{\partial a_1}{\partial w_{22}} \leq 0$ for all $t \in [0, t_f]$. Therefore, the optimal acceleration will decrease with a larger w_{22} , i.e., the second part of Remark 2(i).

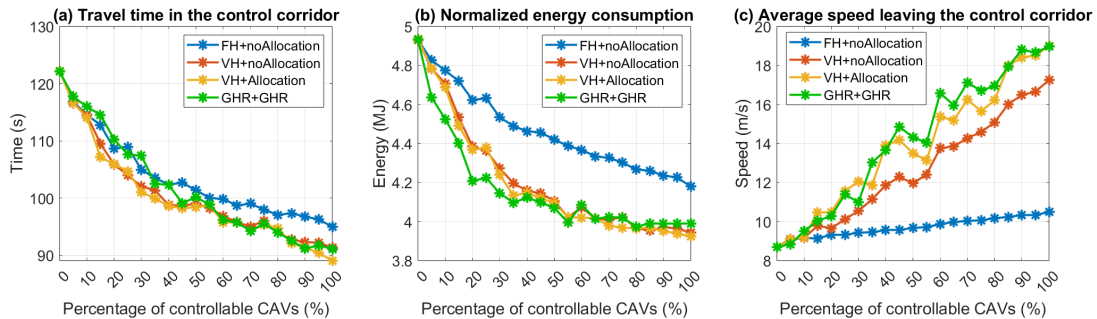


Fig. A2. Comparison of different solution configurations.

Moreover, taking derivative of $a_1(t)$ with respect to τ gives:

$$\begin{aligned} \frac{\partial a_1}{\partial \tau} = & \frac{w_{12}}{2(w_{21} + w_{22})} \cdot \\ & \left[e^{\sqrt{\frac{w_{21}+w_{22}}{\tau^2 w_{21}}}(t-t_f)} \left(1 - \sqrt{\frac{w_{21}+w_{22}}{\tau^2 w_{21}}}(t-t_f) \right) - 1 \right]. \end{aligned} \quad (\text{A19})$$

We can verify that $\frac{\partial a_1}{\partial \tau} \leq 0$ for all $t \in [0, t_f]$, i.e., Remark 2(iv).

It is noteworthy that more following HVs can be considered by improving w_{12} and w_{22} . For simplicity, we assume that all vehicles are assigned the same weighting factors for travel distance and energy consumption, i.e., w_1 and w_2 , respectively. The optimal control of the lead CAV considering n following HVs can be given by:

$$a_1(t) = \frac{w_1}{2w_2}(t_f - t) + \frac{nw_1\tau}{2(n+1)w_2} \left[e^{\frac{\sqrt{n+1}}{\tau}(t-t_f)} - 1 \right] \quad (\text{A20})$$

which decreases with respect to the number of following HVs n . Therefore, considering more HVs, the acceleration would decrease, i.e., Remark 2(v).

This completes the proof. \square

APPENDIX H GREEN WINDOW ALLOCATION ALGORITHM

See Algorithm A1.

APPENDIX I COMPARISON OF SOLUTION APPROACHES

In Section II-C, we propose the varying optimization horizon and the green window allocation algorithm for scenarios with signalized intersections. Then, Section III-A1 evaluates the proposed method in a signalized corridor under different proportions of controllable CAVs. With the same traffic settings as Section III-A1, Fig. A2 shows the numerical results with different solution configurations, i.e., fixed optimization horizon and without green window allocation (FH+noAllocation), varying optimization horizon and without green window allocation (VH+noAllocation), and varying optimization horizon and with green window allocation (VH+Allocation). Moreover, different from Section III, uncontrollable vehicles are simulated by the IDM, but are optimized based on the GHR model), a full-information simulation

Algorithm A1 Green window allocation.

```

1: Input:  $N(t)$ ,  $N_c(t)$ ,  $\mathbf{x}(t)$ 
2: Initialize  $U = \emptyset$ ,  $j = 0$ , and optimization horizon  $[t, t_f]$ 
3: Solve the optimization problem (23) for all vehicles in
    $N(t)$  from  $t$  to  $t_f$ 
4: for  $i \in N_c(t)$  do
5:   if  $d_i(t_f) > d_{sig}$  then
6:     Update  $U = U \cup \{a_i\}$ 
7:   else
8:      $j = i$ 
9:     Break
10:  end if
11: end for
12: if  $j \neq 0$  then
13:    $N'(t) = \{j, j+1, \dots, n(t)-1, n(t)\}$  and  $N'_c(t)$  is the
      set of CAVs in  $N'(t)$ 
14:    $t'_f = t_f + t_r + t_g$ 
15:   Solve the optimization problem (23) for all vehicles in
       $N'(t)$  from  $t$  to  $t'_f$ 
16:   for  $i \in N'_c(t)$  do
17:     Update  $U = U \cup \{a_i\}$ 
18:   end for
19: end if
20: Output:  $U$ 

```

case is also shown in Fig. A2, where car-following behavior of uncontrollable vehicles is simulated by the GHR model (GHR+GHR).

As shown in Fig. A2, although FH+noAllocation (the blue line) can achieve mobility and energy benefits, more benefits are achieved in VH+noAllocation (the red line) as it can make better use of SPaT information by adopting a varying optimization horizon. The green window allocation algorithm can further improve the benefits (the yellow line), especially in the average leaving speed shown in Fig. A2(c). This is because CAVs that cannot pass the intersection during the current green phase will decelerate in advance and target to pass the intersection during the next green phase at a higher speed. Moreover, the full-information case is shown in green. Since the GHR model only considers the speed difference but ignores the following distance of two consecutive vehicles, the GHR model may result in a smaller acceleration of the following vehicle compared with the IDM. For example, the vehicle modeled by the GHR model may not accelerate as long as it has the same speed as its preceding vehicle, even if the following distance is large. The smaller acceleration will lead to less energy consumption but longer travel time. Therefore, compared with yellow lines in Fig. A2(a-b), green lines have less energy consumption, but longer travel time, especially at a low proportion of controllable CAVs. The yellow and green lines always have similar trends, indicating that the proposed method can achieve benefits in traffic and energy efficiency even when the car-following model adopted in optimization is a simplification of the real-world car-following behavior.

APPENDIX JPERFORMANCE OF THE PROPOSED METHOD IN A SCENARIO
WITH UNCERTAINTIES

In this appendix, we test the proposed method in a scenario with uncertainties. Specifically, the acceleration speed (m/s^2) of uncontrollable vehicles is calculated by the IDM added a random value ϵ , i.e., given by (A21). Given that the minimum acceleration and maximum acceleration are $-1.5m/s^2$ and $1m/s^2$, respectively, the random value ϵ is set as following a uniform distribution in the interval $[-0.05, 0.05]$.

$$a_i(t) = a \left[1 - \left(\frac{v_i(t)}{v_0} \right)^\delta - \left(\frac{s^*(v_i(t), \Delta v_i(t))}{s} \right)^2 \right] + \epsilon. \quad (\text{A21})$$

Fig. A3 compares the performance of the proposed method in scenarios with/without uncertainties. Based on the traffic scenario in Section III-A1, The red line and blue line represent the average performance with and without considering uncertainties in the IDM model, respectively. For a fair comparison, the permutations of controllable CAVs keep the same for all 30 simulated cases in each percentage of controllable vehicles. As shown in Fig. A3, when there are traffic oscillations, the throughput of the road may decrease (travel time increases and average leaving speed decreases), especially at a low percentage of controllable vehicles. The normalized energy consumption (solid line) is also higher under uncertainties, where both the tractive energy (dashed line) and the kinetic energy gap (dotted line) are higher under uncertainties shown in Fig. A3(b). Whereas the performances are similar at a high percentage of controllable vehicles because there will be less randomness. Importantly, it can be observed that the proposed method can handle traffic oscillations as it can improve road throughput and reduce energy consumption with a higher percentage of controllable vehicles.

APPENDIX K
PERFORMANCE OF FIRST 18 VEHICLES IN FIG. 5

Table A3 lists the performance of individual vehicles in cases A-D shown in Fig. 5, in terms of the travel time (s), energy consumption (MJ), and average leaving speed (m/s) of each vehicle, respectively. The vehicle indexes are shown in the first column and underlined values are the performance of controllable CAVs. According to the numerical results, the first 17 vehicles can pass the intersection in the same green phase. To save space, only the first 18 vehicles are presented in the table. It can be observed that the controllable CAVs may have smaller energy consumption and can bring energy benefits to their following vehicles. For example, vehicle 4 in cases A-B. Moreover, the controllable CAVs may also have more energy consumption. This is because the CAV will adopt higher acceleration when guiding many vehicles passing the intersection, which is consistent with Remark 2(v). For example, vehicle 1 in cases C-D. The first few vehicles following the accelerating CAV may also have higher energy consumption. However, the whole traffic flow can achieve energy benefits and the road throughput can be improved.

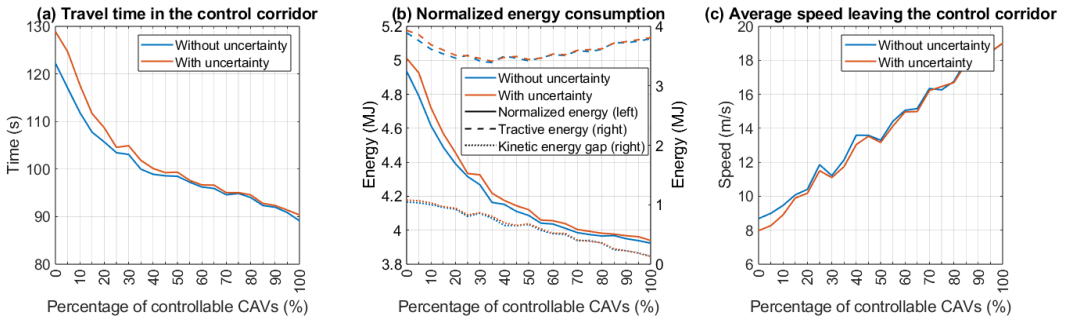


Fig. A3. Performance of the proposed method with uncertainties.

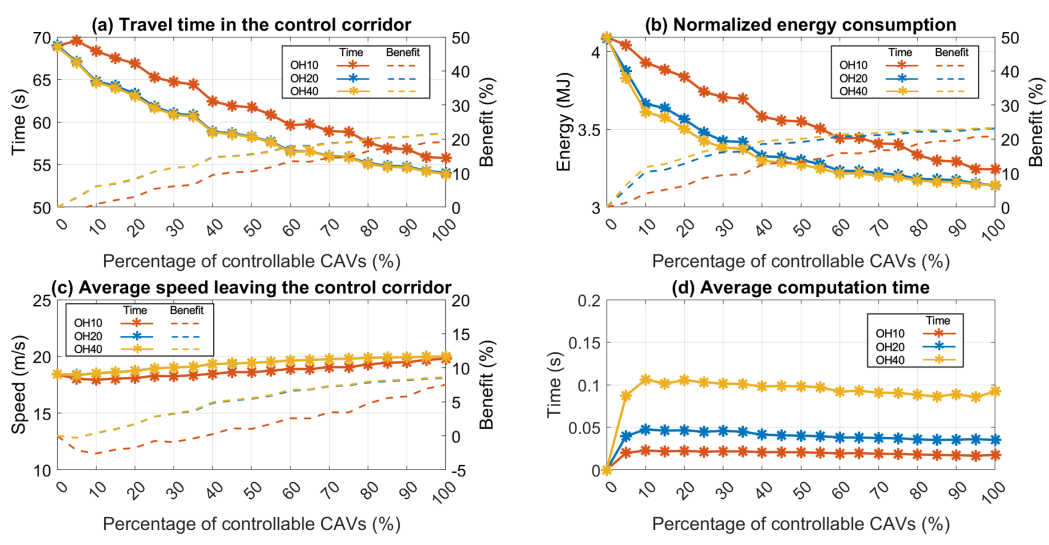


Fig. A4. Comparison of different lengths of the fixed optimization horizon.

Comparing with vehicle 17, the travel time of vehicle 18 is substantially larger because it has to stop at the intersection.

APPENDIX L DIFFERENT OPTIMIZATION HORIZONS

In a corridor without signalized intersections, the proposed method adopts a fixed optimization horizon. The length of the optimization horizon may also affect the performance of the proposed method. To examine this effect, Fig. A4 shows numerical results under different proportions of controllable CAVs with three different lengths of the optimization horizon, i.e., 10s (OH10), 20s (OH20), and 40s (OH40).

Generally, the longer the optimization horizon, the more future states can be optimized at the same time, leading to more benefits. On the contrary, controllable CAVs are myopic with a short optimization horizon. Therefore, as shown in Fig. A4(a) and Fig. A4(c), the travel time increases and the average leaving speed decreases in OH10 at low proportions of controllable CAVs. It is also observed that OH20 is much better than OH10 in reducing travel time and improving the average leaving speed. If the optimization horizon is further extended, the improvement becomes limited, e.g., OH40 has a similar performance to OH20 in Fig. A4(a) and Fig. A4(c). Moreover, as shown in Fig. A4(b), the longer the optimization

TABLE A3
PERFORMANCE OF FIRST 18 VEHICLES IN CASES A-D OF FIG. 5

| No. | Case A | Case B | Case C | Case D |
|-----|---------------------|----------------------|----------------------|----------------------|
| 1 | 126.5/5.0/1.9 | 126.5/5.0/1.9 | 126.7/5.1/9.7 | 126.7/5.1/9.4 |
| 2 | 124.7/4.9/4.1 | 124.6/4.9/4.1 | 122.8/4.9/10.0 | 122.8/4.9/9.6 |
| 3 | 122.7/4.9/5.4 | 121.4/4.8/5.4 | 120.6/4.9/10.4 | 118.3/4.9/9.9 |
| 4 | 117.2/4.7/6.5 | <u>117.5/4.1/6.5</u> | 113.0/4.8/10.6 | 114.9/4.9/10.3 |
| 5 | 113.0/4.7/7.3 | 112.5/4.4/7.4 | 109.1/4.9/11.1 | 109.2/4.9/10.6 |
| 6 | 110.5/4.7/8.1 | 107.0/4.5/8.1 | 103.9/4.8/11.3 | 102.6/4.8/10.9 |
| 7 | 104.7/4.6/8.7 | 104.3/4.5/8.8 | 97.9/4.8/11.7 | 98.9/4.8/11.2 |
| 8 | 99.6/4.6/9.4 | 97.7/4.5/9.5 | 92.0/4.7/11.9 | 91.3/4.7/11.4 |
| 9 | 96.5/4.5/10.0 | 92.7/4.5/10.0 | 87.8/4.6/12.2 | 87.3/4.6/11.7 |
| 10 | <u>90.0/3.7/9.9</u> | 89.6/4.5/10.6 | 82.3/4.4/12.4 | 82.9/4.4/11.9 |
| 11 | 83.6/3.9/10.9 | 85.2/4.4/11.1 | 74.5/4.2/12.7 | 75.9/4.3/12.2 |
| 12 | 79.2/4.0/11.4 | 79.2/4.3/11.6 | 70.5/4.2/12.9 | 71.0/4.2/12.4 |
| 13 | 74.3/4.1/11.9 | 73.3/4.2/12.0 | 65.7/4.0/13.2 | 65.8/4.0/12.7 |
| 14 | 69.3/4.1/12.2 | <u>68.3/3.4/11.1</u> | 58.2/3.4/13.5 | 61.0/3.8/12.8 |
| 15 | 64.4/4.0/12.5 | 62.9/3.4/12.0 | 53.7/3.0/15.7 | <u>55.6/2.8/17.6</u> |
| 16 | 58.3/3.7/12.7 | 57.2/3.3/12.6 | <u>51.7/2.7/20.0</u> | 51.4/2.8/19.4 |
| 17 | 53.4/3.1/15.8 | 53.3/3.1/15.5 | 50.7/2.7/19.9 | 50.3/2.7/19.9 |
| 18 | 148.1/5.2/1.9 | 148.3/5.2/1.9 | 146.9/5.2/1.9 | 147.1/5.3/1.9 |

Note: the numbers in the form of $a/b/c$ represent the travel time (s), energy consumption (MJ), and average leaving speed (m/s) of each vehicle, respectively. The underlined numbers represent controllable CAVs versus others representing uncontrollable vehicles.

horizon, the more benefits in reducing energy consumption. However, as expected, Fig. A4(d) shows that the average computation time increases with the length of the optimization horizon. In this paper, to balance the computation burden and potential benefits, the optimization horizon is set to be 20s for numerical studies in a corridor without signalized intersections.